

Contents lists available at ScienceDirect

# Journal of Quantitative Spectroscopy & Radiative Transfer

journal homepage: www.elsevier.com/locate/jqsrt



# Line mixing and broadening of carbon dioxide by argon in the $v_3$ bandhead near 4.2 $\mu$ m at high temperatures and high pressures



Daniel D. Lee\*, Fabio A. Bendana, Anil P. Nair, Daniel I. Pineda, R. Mitchell Spearrin

Department of Mechanical and Aerospace Engineering, University of California, Los Angeles (UCLA), Los Angeles, CA 90095, USA

# ARTICLE INFO

Article history:
Received 7 February 2020
Revised 1 June 2020
Accepted 2 June 2020
Available online 7 June 2020

Keywords:
Line mixing
Line broadening
Absorption spectroscopy
CO<sub>2</sub>
High pressure
High temperature

#### ABSTRACT

Temperature-dependent line mixing and line broadening parameters were empirically-determined for rovibrational transitions (J=99-145) in the ( $00^00\to00^01$ ) and ( $01^10\to01^11$ ) bandheads of carbon dioxide near 4.2 µm. Collisional effects by argon on the high rotational energy lines ( $E''=3920-8090~cm^{-1}$ ) in the R-branch were studied over a range of temperatures from 1200-3000 K in a shock tube. Measured absorption spectra comprising the target lines in an argon bath gas at near-atmospheric pressures were fit with Voigt profiles to determine line-broadening coefficients, with temperature dependence accounted by a power law. With line broadening established, line-mixing effects were examined at elevated pressures up to 58 atm and similar temperatures, reflecting conditions in high-pressure combustion environments. A modified exponential gap model for line mixing was developed to capture the pressure and temperature dependence of collisional transfer rates for the bandhead region using the relaxation matrix formalism.

© 2020 Elsevier Ltd. All rights reserved.

#### 1. Introduction

Carbon dioxide ( $CO_2$ ) is an important molecule in climatology, biology, planetary astronomy, and combustion chemistry. High-temperature spectroscopy of  $CO_2$  is relevant for remote sensing of extraterrestrial atmospheres [1,2], combustion diagnostics [3], and thermal radiation modeling in the development of planetary entry systems [4,5]. In these applications, quantitative simulation and analysis is enabled by accurate spectroscopic data with appropriate thermodynamic scaling across relevant conditions. This work experimentally investigates the  $CO_2$  spectra near 4.2  $\mu$ m at high-temperature conditions relevant to combustion and propulsion over a broad range of pressures (up to 58.3 atm), with the goal of developing an accurate model of the target spectral domain that accurately captures relevant collisional effects.

The far-wing R-branch transitions of the  $CO_2$  asymmetric stretch  $(\nu_3)$  fundamental bands near 4.2  $\mu m$  have been extensively used for quantitative thermochemical sensing in combustion flows, owing to the high absorptivity and spectral isolation from other combustion species. Researchers have targeted several rovibrational transitions in these bands for  $CO_2$  measurements to char-

E-mail addresses: daniellee9101@ucla.edu (D.D. Lee), fbendana@ucla.edu (F.A. Bendana), anilnair1995@ucla.edu (A.P. Nair), dipineda@ucla.edu (D.I. Pineda), spearrin@ucla.edu (R.M. Spearrin).

acterize scramjet combustor performance [6] (T = 1500-2500 K, P < 2 atm) and spatially-resolve thermochemistry in flames [7-12] (T = 1000-2200 K, P  $\leq$  1 atm). Several shock tube kinetics studies of combustion chemistry have been aided by sensitive time-resolved CO2 species measurements probing this infrared region [13-16] (T = 500-2000 K, P  $\leq$  6 atm). More recently, this spectral domain comprising the bandhead was targeted for inchamber rocket combustion gas sensing at much higher temperatures and pressures (T > 3000 K, P > 50 atm) [17]. At high gas densities, spectrally dense bandhead regions are susceptible to collisional line mixing in addition to broadening [18]. Here we examine line broadening and mixing of CO2 in argon (Ar) for a group of high-energy transitions belonging to the  $v_1v_2^{l_2}v_3(00^00 \rightarrow 00^01)$ and  $(01^10 \rightarrow 01^11)$  bandheads of CO<sub>2</sub> near 4.17 µm. The target domain of interest for line-mixing studies is shown in Fig. 1. The remainder of the manuscript will refer to these regions collectively using a shorthand notation,  $v_3(0 \rightarrow 1)$ .

Many researchers have quantified and modeled  $CO_2$  line broadening for transitions in the  $v_3(0 \rightarrow 1)$  bands, with some reporting broadening effects in Ar [13,19–25], which is often used as a bath gas for chemical kinetics studies in shock tubes. However, to the authors' knowledge no experimentally-measured Arbroadening parameters are reported for rotational quantum number transitions larger than J=100, as indicated in Fig. 2. This is due to most experimental measurements of line broadening coefficients for  $CO_2$  having been conducted below 1000 K, wherein such

<sup>\*</sup> Corresponding author.

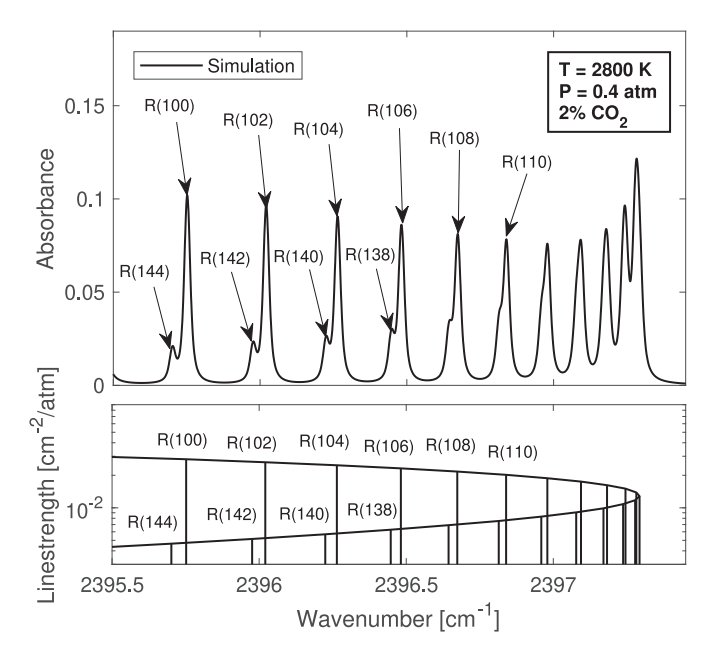


**Fig. 1.** (top) Spectral absorbance simulation of the  $(00^00 \rightarrow 00^01)$  fundamental bandhead of CO<sub>2</sub> at 2800 K and 0.4 atm for 2% CO<sub>2</sub> in air. (bottom) Line positions and magnitudes of the spectral transitions relevant to this work.

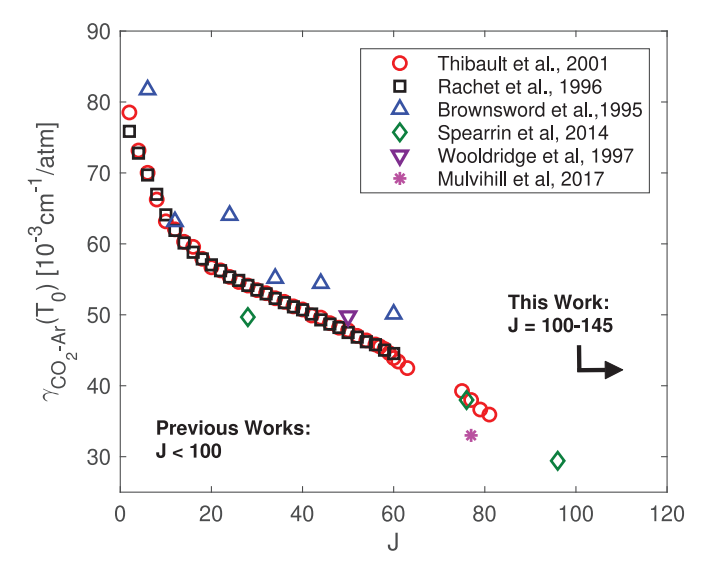


**Fig. 2.** Experimental Ar-broadening coefficients for  $\mathrm{CO}_2$  transitions obtained by previous works for  $T_0=296$  K. The current study focuses on higher rotational quantum number transitions (J=99–145) to extend diagnostic capabilities at extreme temperatures and pressures.

lines are weakly active. We focus this experimental study to 1200–3000 K and evaluate lines with higher rotational energies ( $E''=3920-8090~\rm cm^{-1}$ ).

Line mixing is a band narrowing effect that occurs at high gas densities, resulting from collision-induced changes in rotational energy and is most evident when collisional linewidths are on the order of line spacing [26]. Line mixing within and in the wings of the  $\nu_3$  band of  $\text{CO}_2$  has been investigated previously [22,27–32], owing in part to its relevance in sensing of the Cytherean¹ atmosphere [1], where pressures at the planet surface can exceed 90 atm. Here we study line mixing in the bandhead of the  $\nu_3(0 \rightarrow 1)$  fundamental band of  $\text{CO}_2$  at elevated pressures and very

high temperatures (up to 2850 K) relevant to hydrocarbon-fueled combustion conditions, wherein (similar to broadening) higher rotational energy states are more populated and prior work is absent. This paper describes the experimental measurements and modeling of the aforementioned line broadening and mixing effects in the  $v_3(0 \rightarrow 1)$  fundamental bandhead region of  $CO_2$  at high temperatures and high pressures, with Ar as the collision partner. After establishing the theoretical framework, we present the experimental methods, including the optical setup, shock tube apparatus, and data processing techniques required to obtain broadening and mixing parameters from laser absorption measurements. Broadening parameters are determined at moderate pressures (P < 0.8 atm), where many individual lines can be distinguished. An exponential gap model is then developed to capture line-mixing effects by fitting multi-line absorption spectra at high-pressure conditions (up to 58.3 atm) generated in a shock tube. The broadening and mixing models are shown to enable accurate spectral simulation of CO<sub>2</sub> near 4.2 µm over a broad range of temperatures and pressures.

# 2. Theory

The theory of laser absorption spectroscopy is described thoroughly in the literature [34]. A previous work by our group on line mixing in CO bandhead spectra [35] provides an analogous and more detailed review on the theoretical framework employed for this study. However, since varying definitions and symbols are present in the literature, we provide a brief overview to assist the reader with context and nomenclature definitions.

# 2.1. Absorption spectroscopy and line broadening

The transmission,  $\tau_{\nu}$ , of monochromatic light at frequency,  $\nu$ , through a uniform absorbing gas medium is expressed by the Beer-Lambert law in Eq. (1):

$$\tau_{\nu} = \left(\frac{I}{I_o}\right)_{\nu} = \exp(-\alpha_{\nu}) \tag{1}$$

where  $I_0$  and I are the incident and transmitted light intensities, respectively, and  $\alpha_{\nu}$  is the spectral absorbance. In the spectral vicinity of *a single transition*, the spectral absorbance relates to thermophysical gas properties through Eq. (2):

$$\alpha_{\nu} = S(T)NL\phi(\nu) \tag{2}$$

where S(T) [cm<sup>-1</sup>/(molec · cm<sup>-2</sup>)] is the line strength of the transition, L [cm] is the path length,  $\phi(\nu)$  [cm] is the line shape function, and N [molec · cm<sup>-3</sup>] is the total number density of the absorbing species, given by:

$$N = \frac{PX}{k_B T} \cdot 10^{-6} \tag{3}$$

Here, P is the pressure with units of [Pa], X is the mole fraction of the absorber,  $k_B$  [J/K] is the Boltzmann constant, and T [K] is the temperature. Based on the compressibility factors for  $\mathrm{CO}_2$  and Ar, deviations from the ideal gas assumption implied in Eq. (3) are not expected to exceed 0.4% for any condition in this study [36]. We model the spectral line shape,  $\phi(\nu)$ , using a Voigt profile [26], a convolution of a Lorentzian and a Gaussian profile accounting for collisional and Doppler broadening, respectively. For the Voigt line-shape, both collisional and Doppler broadening are characterized by full width at half maximum (FWHM) parameter;  $\Delta\nu_C$  [cm $^{-1}$ ] for collisional broadening and  $\Delta\nu_D$  [cm $^{-1}$ ] for Doppler broadening. Doppler linewidth is given by Eq. (4) [34]:

$$\Delta \nu_D = \nu_0 (7.1623 \cdot 10^{-7}) \sqrt{\frac{T}{M}} \tag{4}$$

where  $v_0$  [cm<sup>-1</sup>] is the transition linecenter and M [g·mol<sup>-1</sup>] is the molecular weight of the absorbing species. Collisional width

<sup>&</sup>lt;sup>1</sup> The word *Venusian* is also occasionally used to describe properties or behavior pertaining to the planet Venus [33].

scales with the collision frequency of the absorbing molecule *A* (adjusted for quantum state), and is modeled as the product of pressure and the sum of mole fraction weighted collisional broadening coefficients of each perturbing species *B*:

$$\Delta \nu_C = P \sum_B X_B 2 \gamma_{A-B}(T) \tag{5}$$

where  $\gamma_{A-B}(T)$  [cm<sup>-1</sup>atm<sup>-1</sup>] is the transition-dependent collisional broadening coefficient at temperature, T. Note that in Eq. (5), total pressure, P, has units of [atm].

As shown in Eq. (5), collisional broadening scales with pressure linearly. The temperature dependence of  $\gamma_{A-B}(T)$  is modeled as a power law expression:

$$\gamma_{A-B}(T) = \gamma_{A-B}(T_0) \left(\frac{T_0}{T}\right)^{n_{A-B}} \tag{6}$$

where  $\gamma_{A-B}(T_0)$  [cm<sup>-1</sup>atm<sup>-1</sup>] is the broadening coefficient at a reference temperature,  $T_0$ , and  $n_{A-B}$  is the line-specific temperature exponent of the absorbing species. As lines become more closely spaced together or pressure increases, the spectral absorbance,  $\alpha_{\nu}$ , at a given wavenumber,  $\nu$ , is no longer a function of just one spectral transition, but is rather a summation of all neighboring transitions as demonstrated in the bandhead shown in Fig. 1. In this work, we measure values of  $\gamma_{{\rm CO}_2-Ar}$  over a range of temperatures (1200-3000 K) and sub-atmospheric pressures to distinguish 17 transitions within the range of J = 99-145. Transitions are probed in both the  $(00^00 \rightarrow 00^01)$  and  $(01^10 \rightarrow 01^11)$  fundamental bands, recognizing weak vibrational dependence. For each transition, a power law fit with temperature is used to infer  $n_{CO_2-Ar}$  and we report  $\gamma_{\text{CO}_2-Ar}(T_0)$  at a reference temperature of  $T_0=1200$  K. The parameters for inaccessible (overly blended) lines are determined via interpolation.

# 2.2. Line mixing

Line mixing is a phenomena in which molecular collisions induce a change in rotational energy, typically within a given vibrational energy level. These collision-induced transfers between rotational energy states result in an intensity exchange between neighboring transitions and often leads to a vibrational band narrowing effect [26], which enhances high-absorbing regions. This effect scales with collision frequency (or pressure) and is pronounced in spectrally dense regions, such as bandheads, where line spacing is small. An illustration of the line mixing process for two rovibrational transitions is depicted in Fig. 3.

In modeling line-mixing effects, we utilize the relaxation matrix formalism [37], which accounts for aggregate collisional effects (broadening and mixing) on the molecular spectra. In the following equations and figures, J and K refer to transitions between lower and upper states  $J'' \rightarrow J'$  and  $K'' \rightarrow K'$ , wherein the state space is generally distinguished from the line space here with the use of prime (') and double prime (") symbols. We express the absorbance,  $\alpha_{\nu}$ , for overlapping transitions, within the impact approximation [38], in the following form:

$$\alpha_{\nu} = \frac{NL}{\pi} \operatorname{Im}(\mathbf{d} \cdot \mathbf{G}^{-1} \cdot \boldsymbol{\rho} \cdot \mathbf{d}) \tag{7}$$

where  $\rho$  is a diagonal matrix with nonzero elements defined by the lower state Boltzmann population fraction and  $\mathbf{d} [\mathrm{cm}^{-1}/(\mathrm{molec} \cdot \mathrm{cm}^{-2})]^{\frac{1}{2}}$  is a vector describing transition amplitudes. Another equivalent form of Eq. (7) is shown in the Appendix of Bendana et al. [35].

The dependence on wavenumber,  $\nu$  [cm<sup>-1</sup>], in Eq. (7) is within **G** [cm<sup>-1</sup>], a complex matrix defined as:

$$\mathbf{G} = \nu \mathbf{I} - \mathbf{v}_0 - iP\mathbf{W} = \nu \mathbf{I} - \mathbf{H} \tag{8}$$

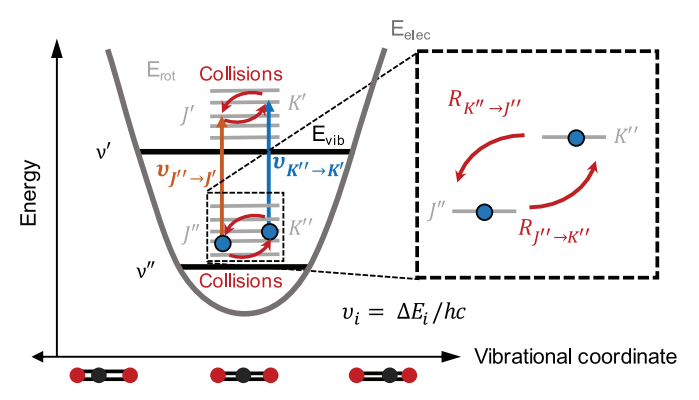


Fig. 3. Collisional line mixing of rovibrational transitions in a fundamental asymmetric stretch band of a linear polyatomic molecule, adapted from Hartmann [26].

where **I** is the identity matrix,  $v_0$  [cm<sup>-1</sup>] is a diagonal matrix of transition frequencies, and **W** [cm<sup>-1</sup>/atm] is the relaxation matrix [37]. In Eq. (8), total pressure, P, is in units of [atm]. The frequency-independent matrix, **H**, can be diagonalized by a matrix **A** using a similarity transform [39] to obtain a diagonal eigenvalue matrix with diagonal elements,  $\omega_J$  [cm<sup>-1</sup>]. Since **G** differs from **H** only by a constant diagonal matrix,  $\mathbf{G}^{-1}$  is also diagonalized by **A**. Eq. (7) can now be written as a function of v summing over all equivalent lines, J:

$$\alpha_{\nu} = \frac{NL}{\pi} \operatorname{Im} \left[ \sum_{J} \frac{(\mathbf{d} \cdot \mathbf{A})_{J} (\mathbf{A}^{-1} \cdot \boldsymbol{\rho} \cdot \mathbf{d})_{J}}{(\nu - \omega_{J})} \right]$$
(9)

We capture line-mixing effects with a relaxation matrix, which is given by:

$$\mathbf{W}_{JK} = \begin{cases} \gamma_J - i\Delta \nu_{0,J} & if \ J = K \\ -A_{RR}R_{J'' \to K''} & if \ J \neq K \end{cases}$$
 (10)

where the real diagonal elements of **W** are the broadening coefficients,  $\gamma_J$ , discussed previously (Section 2.1) and the imaginary diagonal elements are the pressure shifts,  $\Delta \nu_{0J}$  [cm<sup>-1</sup>/atm]. The imaginary off-diagonal components of **W** represent contributions from rovibrational dephasing [40], which can be approximated as zero, and the real off-diagonal elements are approximated by the state-specific population transfer rates  $R_{J'' \to K''}$  [cm<sup>-1</sup>/atm] multiplied by a scaling factor  $A_{RR}$  [26].

Since collisions generally promote the Boltzmann distribution of population, the reciprocal population transfer rates,  $R_{J'' \to K''}$  and  $R_{K'' \to J''}$ , respectively, are related through the detailed-balance principle [41]. If the off-diagonal elements of the relaxation matrix,  $W_{JK}$ , are set to zero, Eq. (7) simplifies to the sum of the Lorentzian lines with no line-mixing effects. Invoking the random phase approximation [24], broadening coefficients can be related to the state-to-state population transfer rates (R) between lower and upper states [26]:

$$\gamma_{J} = \frac{1}{2} \left[ \sum_{J'' \neq K''} R_{J'' \to K''} + \sum_{J' \neq K'} R_{J' \to K'} \right]$$
 (11)

This equation assumes negligible dephasing contributions from elastic collisions [42].

For multiple collision partners, the full relaxation matrix is expressed as a summation of the individual perturber contributions:

$$\mathbf{W} = \sum_{R} X_{B} \mathbf{W}_{A-B} \tag{12}$$

We model the real off-diagonal elements of W with a modified-exponential-gap (MEG) law [43,44] with the form:

$$W_{JK} = a_1(T) \left[ \frac{1 + a_4 \left( \frac{E_J''}{a_2 k_B T} \right)}{1 + a_4 \left( \frac{E_J''}{k_B T} \right)} \right]^2 \times \exp \left[ \frac{-a_3 \left( E_K'' - E_J'' \right)}{k_B T} \right]$$
(13)

where  $a_1(T)$  [cm<sup>-1</sup>/atm],  $a_2$ , and  $a_3$  are species-specific MEG law coefficients obtained by fitting measured absorbance data to the model using a nonlinear least-squares fitting routine.  $a_4$  describes the collision duration [43] based on distance of closest approach [45] and for this study is set to  $a_4=2$  as an estimate for collisions of linear molecules [35]. The MEG law formulation described here has been successfully implemented for several linear molecules [35,46,47], including CO<sub>2</sub> [48,49]. Though some of these studies have used different  $a_4$  values, the sensitivity of  $a_4$  has been tested using  $a_4=1$  and  $a_4=1.5$  and found to have negligible influence on the results [46,48].

The species-specific MEG law coefficients at a given temperature can be obtained by fitting absorbance spectra [50].  $a_1(T)$  can be modeled as a power law expression to determine the temperature dependence of the relaxation matrix components:

$$a_1(T) = a_1(T_0) \left(\frac{T_0}{T}\right)^m$$
 (14)

where  $a_1(T_0)$  is the MEG law coefficient at a reference temperature,  $T_0$ , and m is defined as the temperature exponent, obtained by fitting multiple sets of absorbance data over a range of temperatures.

Similar to the reported broadening coefficients,  $\gamma_{\text{CO}_2-Ar}$ , we report measured values of MEG law coefficients for  $a_i$  and the associated temperature exponent, m, at a reference temperature of  $T_0=1200$  K. We show that these parameters can be used to accurately model line-mixing effects in the  $(00^00 \rightarrow 00^01)$  bandhead of CO<sub>2</sub> near 4.17  $\mu$ m at high pressures (10–60 atm) over a temperature range of 1200–3000 K.

# 3. Experimental methods

The experiments in this work were conducted using a highenthalpy shock tube facility [35,51]. We provide a brief description here for context and reader clarity. The shock tube and corresponding optical setup are illustrated in Fig. 4. All laser absorption measurements are attained behind reflected shock waves that near-instantaneously heat a prescribed gas mixture to target conditions for a short test time (milliseconds). Initial reflected shock conditions are determined by measurements of the incident shock speed and normal shock relations, yielding a typical uncertainty of  $\sim 1\%$  in temperature when properly accounting for vibrational relaxation of the gas mixture [52]. Prior to each experiment, a roughing pump (Alcatel Adixen 2021i) was used to vacuum down the shock tube to  $< 1 \times 10^{-3}$  Torr. Test gas mixtures were barometrically prepared in a 12.5 L agitated mixing tank using a heated capacitance manometer (MKS 627D Baratron) with a full-scale pressure range of 1000 Torr and an uncertainty of 0.12% of the reading. At higher pressures, an additional pressure transducer (Setra GCT-225) with an accuracy of 0.25% of the full scale (1000 psi) was used to prepare mixtures. All gases were supplied by Airgas, Inc. with purity levels of 99.999% for CO<sub>2</sub>, 99.999% for Ar, and 99.995% for N2 and He. Different mixtures were prepared for collisional broadening and line mixing investigations (2%–5% CO<sub>2</sub>/Ar) depending on the expected intensity of the transitions being measured; higher concentrations of CO2 were used for the higher J lines to increase absorbance and measurement signal-to-noise. Different driver gases (either N2 or He) and diaphragm thicknesses were used depending on the reflected shock conditions desired.

Two continuous-wave (CW) distributed feedback (DFB) interband cascade lasers (Nanoplus) were utilized to spectrally-resolve the mid-infrared  $CO_2$  spectra. Each ICL has approximately  $\sim 3$  mW output power, and is rapidly tunable via injection current. One ICL targeted the primary domain of interest near 4.17 µm (2395-2398 cm<sup>-1</sup>) to study lines near the  $(00^00 \rightarrow 00^01)$  bandhead. As seen in Fig. 1, this spectral region consists of even J = 100-144. As is common in bandheads, many of these lines are blended together even at moderate pressures ( < 0.5 atm), precluding distinct broadening measurements for several lines. To build a more comprehensive broadening dataset and establish a I-dependence, additional CO<sub>2</sub> transitions from the neighboring  $(01^10 \rightarrow 01^11)$  band with similar J (99-145) were also evaluated using an ICL near  $4.19 \ \mu m \ (2383-2385 \ cm^{-1})$ . It should be noted that vibrational dependence of broadening is expected to be less than 2% [53,54] and, as a result, was considered negligible. While the two aforementioned bands were targeted for broadening measurements of similar high J lines, only the  $(00^00 \rightarrow 00^01)$  bandhead near 2398 cm<sup>-1</sup> was investigated for line mixing. To confirm that CO2 did not dissociate into CO during the shock-heated experiments, we also used a quantum cascade laser (QCL, ALPES) centered at 4.98 µm targeting the P(0,31) and P(2,20) transitions in the CO fundamental bands

The interband cascade lasers were injection current tuned with 10 kHz triangle waveforms, shown in Fig. 4, over a wavenumber range of  $\sim 1.6 \text{ cm}^{-1}$  at various intervals between 2382–2400 cm<sup>-1</sup>. Similarly, the QCL targeting CO was tuned over a wavenumber range of  $\sim 1.2~\text{cm}^{-1}$  between 2008–2009  $\text{cm}^{-1}$  at a similar frequency. For all lasers, the injection current was scanned below the lasing threshold to account for transient thermal emission during the measurements. The relative frequency of the laser light during the scan was determined using a germanium etalon with a free spectral range of 0.0231 cm<sup>-1</sup>. During the experiments, the incident light was pitched through a CaF2 beamsplitter and across the shock tube through two 0.5° wedged sapphire windows with a 9.5 mm aperture, as shown in Fig. 4. The transmitted light was again passed through a beamsplitter, followed by a bandpass spectral filter (Electro Optical Components, 4210 ± 42 nm or Spectrogon,  $4960 \pm 148$  nm) to separate the two light sources. After the spectral filters, the light from each respective wavelength passed through an iris to mitigate thermal emission, and was focused onto a thermo-electrically cooled photodetector (Vigo PVI-4TE-5) using a CaF<sub>2</sub> plano-convex lens. Incident and reflected shock pressures were measured by a dynamic pressure transducer (Kistler 601B1) mounted in one of the test section ports and connected to a charge amplifier (Kistler 5018A). Pressure and detector data were collected on a PicoScope 4000 series data acquisition module at 80 MHz while detector data were sampled at the maximum detector bandwidth of 10 MHz, yielding an equivalent measurement rate of 5 MHz.

Representative raw time-resolved signals from a shock tube experiment are shown in Fig. 4. Following the passage of the incident and reflected shocks, the target lines appear as the high temperatures more densely populate the high J'' rotational energy levels. During the experiment, a non-ideal pressure rise was occasionally observed and accounted for by assuming isentropic compression of the test gas [35]. This assumption has been validated as an accurate method for correcting thermodynamic conditions behind reflected shock waves [55]. For a single scan interval, the change in temperature and pressure are less than 0.75% and 0.5%, respectively; thus, the thermodynamic properties were assigned at the scan mid-point and assumed to be constant during each scan.

Shock tube experiments for Ar line broadening parameters of CO<sub>2</sub> were conducted over a temperature range of 1200–3000 K and a pressure range of 0.352–0.804 atm. Moderate pressures were targeted for line-broadening experiments to minimize spectral blend-

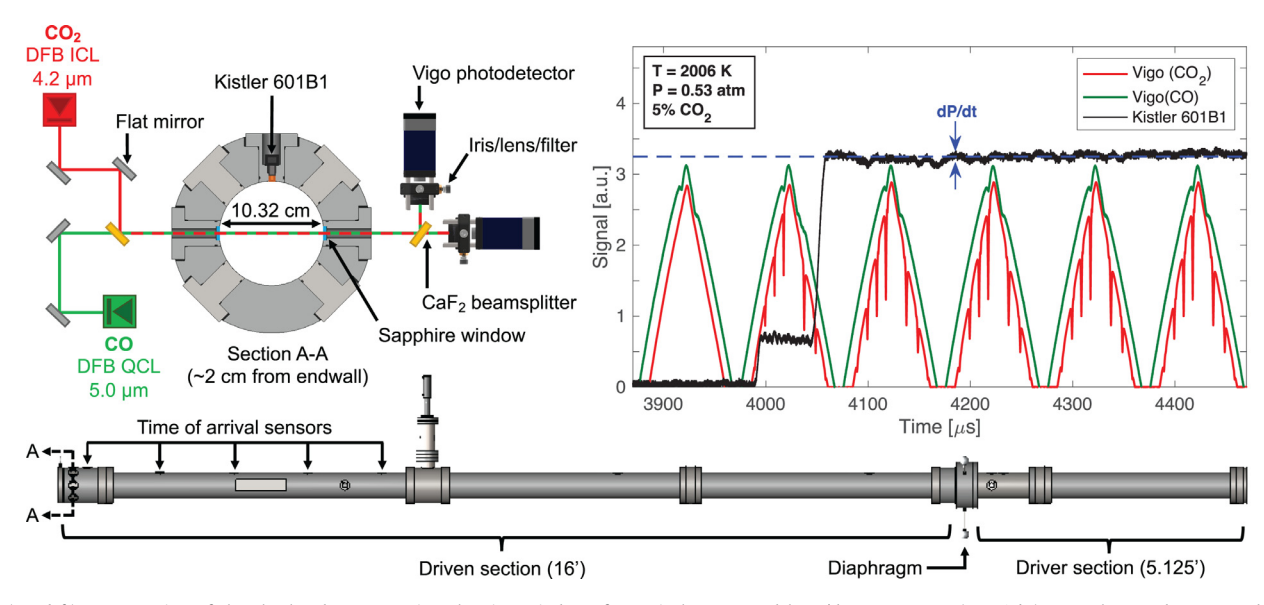


**Fig. 4.** (top left) Cross-section of the shock tube test section showing windows for optical access and laser/detector setup. (top right) Example raw detector and pressure transducer signals during non-reactive shock heating of 5% CO<sub>2</sub> in Ar. (bottom) Side view of the shock tube showing lengths of the driven and driver sections of the tube as well as the locations of the time-of-arrival sensors.

**Table 1** Ar-broadened line parameters for the CO<sub>2</sub>  $\nu_3(0 \rightarrow 1)$  bands.

Transition $(v_3'', J'')$	$\gamma_{\text{CO}_2-Ar}(1200 \text{ K})$ [ $10^{-3} \text{ cm}^{-1} \text{atm}^{-1}$ ]	$n_{{\rm CO}_2-Ar}$
R(0,100)	$15.26 \pm 0.63$	$0.466 \pm 0.012$
R(0,105)	$14.80 \pm 0.55^{a}$	$0.454 \; \pm \; 0.014^{a}$
R(0,110)	$14.34 \pm 1.18$	$0.442 \pm 0.024$
R(0,115)	$13.88 \pm 1.38^{a}$	$0.430 \pm 0.023^{a}$
R(0,120)	$13.42 \pm 1.23^{a}$	$0.418 \pm 0.040^{a}$
R(0,125)	$12.96 \pm 1.19^{a}$	$0.406 \pm 0.039^{a}$
R(0,130)	$12.50 \pm 1.15^{a}$	$0.394 \pm 0.038^{a}$
R(0,135)	$12.04 \pm 1.01^{a}$	$0.382 \pm 0.053^{a}$
R(0,140)	$11.58 \pm 0.92$	$0.370 \pm 0.053$
R(0,145)	$11.12~\pm~0.68$	$0.357 \; \pm \; 0.024$

<sup>&</sup>lt;sup>a</sup> Interpolation based on J-dependence (reference Fig. 7)

ing amongst neighboring transitions and resolve the line-specific broadening and temperature coefficients discussed in Section 2.1. Shock tube experiments for line-mixing parameters covered a temperature and pressure range of 2000–3000 K and 16.5–58.3 atm, respectively. Higher pressures were targeted for line-mixing experiments in order to determine MEG law coefficients and prove pressure scalability. A complete test matrix of all the experimental conditions for these measurements can be found in the Supplementary Material.

For each experiment, absorbance,  $\alpha_{\nu}$ , was determined through Eq. (1) via measurements of incident and transmitted intensity,  $I_0$  and I. The incident laser light intensity through the shock tube was measured without a mixture present prior to each shock experiment to provide a baseline  $I_0$  for calculation of  $\alpha_{\nu}$ . Each scan of the transmitted laser intensity, I, was corrected for detector offset from both emission and dark current noise by tuning below the lasing threshold. Minimal emission was observed throughout the tests, as seen in the representative data from Fig. 4. To obtain line-broadening coefficients, the measured absorbance spectra for a group of transitions (regions identified in Fig. 5) was least-squares fit with Voigt lineshape functions with broadening coefficient,  $\gamma(T)$ , and line position,  $\nu_0$ , set as the free parameters. It should be noted that since the fit was performed on a group of transitions, the relative line position is critical; therefore,

the bounds for  $\nu_0$  were determined by uncertainties in the etalon measurement. X, T, P, and L were held constant and determined from the barometric mixture preparation, reflected shock conditions, and shock tube geometry. The minor self-broadening from  $CO_2$  was also included in the simulation, effectively correcting for this contribution. For higher-pressure line-mixing experiments, the MEG law coefficients were set as free parameters with the diagonals of the relaxation matrix assigned with the pre-determined broadening coefficients.

# 4. Results and discussion

Temperature dependent line-broadening coefficients of  $CO_2$  with Ar are reported for transitions in the range of J=99–145, suitable for spectral modeling over a temperature range of 1200–3000 K. Seventeen transitions are measured directly through line fitting, while the remainder are inferred via interpolation (and compared with measured spectra). Line mixing coefficients are also reported for the  $(00^00 \rightarrow 00^01)$  bandhead region near 2395–2398 cm<sup>-1</sup> to capture the spectral distortion effects at pressures up to 58 atm and similarly high temperatures. The following two subsections detail the line-broadening and line-mixing results, respectively.

# 4.1. Line broadening

As described in Section 3, scanned-wavelength laser absorption measurements were made behind reflected shocks to gather  $CO_2$  spectral data from 1200–3000 K. Representative single-scan absorbance measurements from shock tube experiments with corresponding Voigt line fits are shown in Fig. 5 for the spectral regions (A, B, and C) evaluated in this work. As indicated and aforementioned, measurements were conducted in two different bands to empirically-determine Ar-broadening parameters for rovibrational transitions in the range of J=99-145. The primary motivation of this work was to accurately model the  $(00^00 \rightarrow 00^01)$  bandhead region near 2395–2398 cm<sup>-1</sup> over a wide range of temperatures and pressures. However, fitting individual lines in this domain proved difficult due to severe overlap near the bandhead. As such, distinct line fits in the  $(00^00 \rightarrow 00^01)$  band were restricted to Region

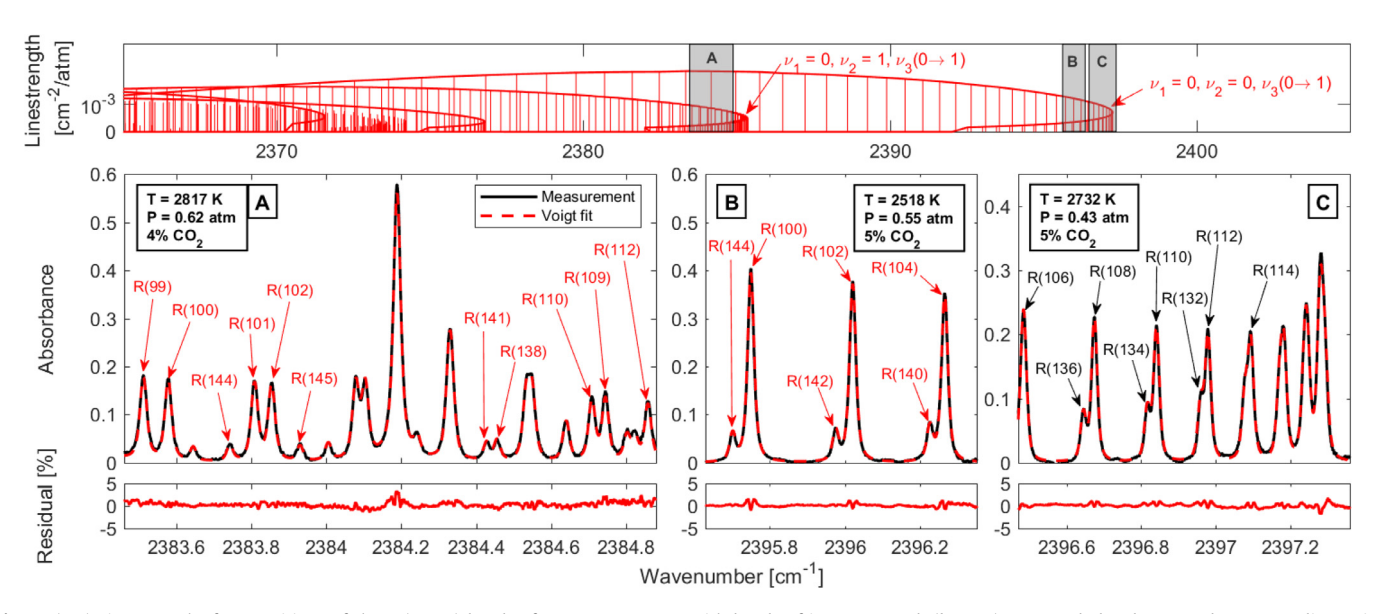


Fig. 5. (top) Linestrengths for transitions of the  $v_3(0 \rightarrow 1)$  bands of CO<sub>2</sub> near 4.2  $\mu$ m, with bands of interest noted. (bottom) Measured absorbance and corresponding Voigt fits for the transitions shown, using the broadening parameters reported in Table 1. Transitions with broadening parameters directly measured in this work noted in red, while those with inferred parameters are noted in black.

B, near 4.17  $\mu$ m, which included only 6 of the 22 lines of interest (note only even J are allowed in this band). Despite the dataset including transitions before and after the bandhead (higher and lower J), the sparse number of lines was deemed insufficient to infer the parameters of the intermediate J. Accordingly, an additional 11 transitions near 4.19  $\mu$ m were distinctly measured from the  $(01^10 \rightarrow 01^11)$  band, shown in Fig. 5 Region A. This region similarly includes a number of other lines that could not be fit reliably due to severe overlap or weak absorbance and are excluded in subsequent data analysis. The 17 lines from which fitting parameters were used are labeled in red by their lower state rotational quantum number in Fig. 5.

Region C in Fig. 5 shows a comparison between a low-pressure measurement of the blended ( $00^00 \rightarrow 00^01$ ) bandhead and a simulation using the line broadening parameters which were interpolated based on the measurements from Regions A and B. Details regarding the data analysis process to obtain these results are discussed here. Generally, the Voigt fits of lines in Regions A and B produced low peak residuals (1-2%). At high temperatures and moderate pressures the Ar-broadened spectra exhibited some evidence of collisional narrowing (gull-wing residual) [56], but the signal-to-noise ratio was deemed insufficient to rigorously evaluate more advanced lineshapes than the Voigt (which performed quite well). In order to accurately determine Ar-broadened line parameters from the Voigt fits, the contribution from selfbroadening, calculated from the line parameters reported in the HITEMP database [57], have been subtracted from the measured collision widths.

Fig. 6 shows the  $\mathrm{CO}_2$ -Ar broadening coefficient versus temperature for a subset of transitions before and after the bandhead, representing all relevant temperature conditions. The measured broadening coefficients were fit with a power law to obtain a temperature dependence,  $\gamma(T)$ , for each transition. It can be noted that at the lower temperatures, the highest J lines could not be reliably discerned, reducing the number of data points available to the power law fit. To help reduce uncertainty in the temperature dependence for the lines measured in this work and constrain the power law fits, we incorporate estimates of  $\gamma_{\mathrm{CO}_2-Ar}$  at 765 K by performing a linear regression of data reported by Thibault [24] measured for lower J transitions [58]. More detail on

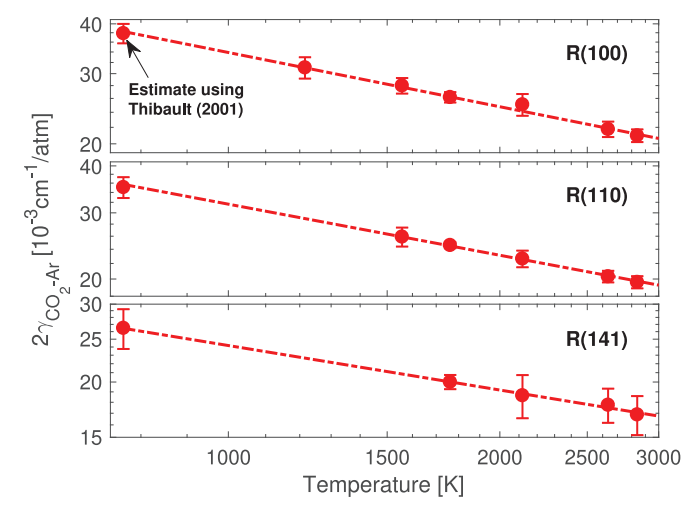
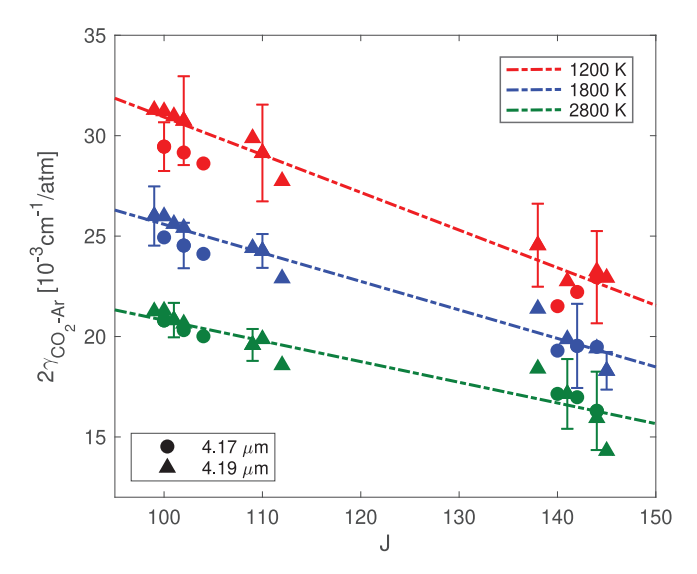


Fig. 6. Ar-broadening coefficients for the transitions of interest with power law fits for  $765-3000\ K$ .

the calculation of these estimates and their associated uncertainties is provided in Appendix A. Subsequently, the  $\gamma(T)$  values for each measured transition were used in a linear regression to estimate the relationship between  $\gamma(T)$  vs J, shown as dash-dotted lines in Fig. 7, for different temperatures.

As discussed previously, line-broadening experiments targeted lower pressures ( < 0.8 atm) to minimize spectral blending from neighboring transitions, which become more significant near the bandhead and complicates the spectral fitting. Despite utilizing multiple bandheads and the low pressures of the experiments, the R(113)–R(137) transitions are too closely spaced and blended to reliably fit and extract broadening information. Accordingly, we infer broadening coefficients for these lines via the linear interpolation, as indicated in Fig. 7. The linear relationship between  $\gamma_{\text{CO}_2-Ar}$  [cm<sup>-1</sup>/atm] and J at temperature 1200 K can be expressed with the following equation:

$$\gamma_{\text{CO}_2-Ar}(1200 \text{ K}) = 0.025 - 9.205 \times 10^{-5} \text{ (J)}$$
 (15)



**Fig. 7.** Measured broadening coefficients  $2\gamma_{\text{CO}_2-Ar}$  (markers) for J=99–145 for 1200 K (red), 1800 K (blue), and 2800 K (green). Least-squares exponential fits (lines) of the measured (filled markers) are used to estimate  $2\gamma_{\text{CO}_2-Ar}$  for J too interfered to measure directly. Representative error bars shown for plot clarity.

Temperature-dependent exponents  $n_{\text{CO}_2-Ar}$  for all measured and interpolated transitions are determined by similarly fitting the inferred broadening coefficients  $\gamma_{\text{CO}_2-Ar}(T)$  over the range of test temperatures. The resulting values of  $n_{\text{CO}_2-Ar}$  can be modeled as a function of J using the following equation:

$$n_{\text{CO}_2-Ar} = 0.708 - 2.417 \times 10^{-3} (J) \tag{16}$$

Note this expression is only considered suitable for J=99-145. The corresponding broadening parameters for select transitions and their uncertainties are listed in Table 1 with a reference temperature of  $T_0=1200$  K. Superscripts in the table indicate if the reported parameter is from an interpolated transition. Power-law fits of all measured broadening coefficients versus temperature (similar to the subset shown in Fig. 6) are provided in the Supplementary Material to support these summary results. The values in Table 1 and predicted by Eq. (16) are considered most appropriate for a temperature range T=1200-3000 K.

Revisiting Fig. 5, it can be noted that the interpolated broadening parameters in Region C, when coupled with a Voigt lineshape simulation, yield excellent agreement with measured spectra. The spectra in Region C exhibits very low residuals ( < 2%) despite the indirect inference using data from Regions A and B. The slightly more pronounced discrepancy at the bandhead near 2397.3 cm<sup>-1</sup> provides evidence of line-mixing effects even at these lower pressures [7,9].

# 4.2. Line mixing

As discussed in Section 2.2, the relaxation matrix,  $\mathbf{W}$ , accounts for the collision-induced population transfer rates that determine line mixing and narrowing effects in the molecular spectra. The real diagonal elements of  $\mathbf{W}$  are the broadening coefficients,  $\gamma_J$ , the imaginary diagonal elements are the pressure shifts,  $\Delta \nu_{0J}$ , the real off-diagonal elements are proportional to the state-specific population transfer rates,  $R_{J'' \to K''}$ , and the imaginary off-diagonal components are approximated as zero. The reported broadening coefficients in Table 1 and pressure shift coefficients from the HITEMP database [57] are used to complete the real and imaginary diagonal elements of  $\mathbf{W}$ , respectively. Though the HITEMP database only provides  $\mathrm{CO}_2$ -air pressure shift coefficients, deviations from this assumption were found to negligibly affect the fitting results.

The real off-diagonal elements were obtained through the MEG law, described by Eq. (13), and the detailed balance principle for a grouping of 34 transitions from J=88-154. To find the MEG law coefficients,  $a_i$ , high pressure absorbance data measured using the shock tube facility are least-squares fit with the absorbance model given by Eq. (7), with  $a_1$ ,  $a_2$ , and  $a_3$  set as the free parameters. This procedure was carried out with test gas mixtures of 2% CO<sub>2</sub>/Ar to obtain the appropriate rates for CO<sub>2</sub>-Ar collisions using Eq. (12).

A comparison of representative high-pressure absorbance data collected in the shock tube at 36 atm and 2493 K is shown in Fig. 8 with various simulations. The measured data is compared to simulated results using the line-mixing model developed in the present work and a model developed by Lamouroux et al [32] for CO2 line mixing in air based on the HITRAN 2016 database [58]. Notably, the air-broadened line-mixing model based on HITRAN 2016 poorly represents the measured spectra at all wavenumbers of interest; the disagreement is largely due to several missing high J transitions, which are included in the HITEMP database [57]. Using the HITEMP database with the updated Ar-broadening parameters reported in Table 1 yields a prediction closer to the measurement; however, without considering line mixing, the simulated spectra significantly underpredicts absorbance near the bandhead, where pronounced narrowing occurs. Implementing the aforementioned MEG law fitting routine enables a highly accurate reconstruction of the spectra with residual < 3%. This compares to a disagreement of nearly 30% at the bandhead peak without accounting for line mixing. Notably, away from the bandhead, the line mixing model still agrees well with both the measured absorbance and converges to simulated spectra that ignores line mixing. To illustrate the sensitivity to the MEG law coefficients, we adjust the  $a_1$  parameter ( + 45%) to vary the degree of line mixing and visualize the associated changes in the spectra. As population transfer rates increase, line mixing favors intensity transfers from weak absorption regions to strong absorption regions, consequently narrowing the spectral structure and increasing the differential absorption near the bandhead

It is informative to compare the transfer rates of different transitions as a function of  $\Delta J$ . Fig. 9 shows the real off-diagonal ele-

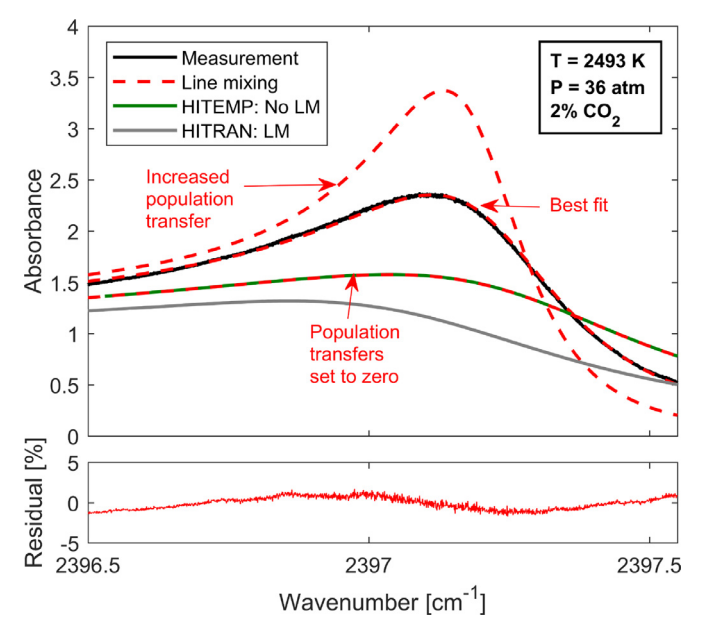


**Fig. 8.** Absorbance measurement of the  $(00^00 \rightarrow 00^01)$  fundamental bandhead of CO<sub>2</sub> at 2493 K and 36 atm with spectral simulations using Eq. (2) (green), Eq. (7) (red) with varying magnitude of population transfer rates, including no population transfers  $(a_1 = 0)$ , and the line mixing (LM) model developed by Lamouroux et al [32] available in the HITRAN database [58] (grey).

**Table 2**Temperature-dependent MEG law parameters determined in this work.

	a <sub>1</sub> (1200 K) [10 <sup>-3</sup> cm <sup>-1</sup> atm <sup>-1</sup> ]	$a_2$	$a_3$	$a_4$	m
CO <sub>2</sub> -Ar	$53.94 \pm 2.49$	$4.98~\pm~0.25$	$3.19~\pm~0.13$	2	$2.06~\pm~0.07$

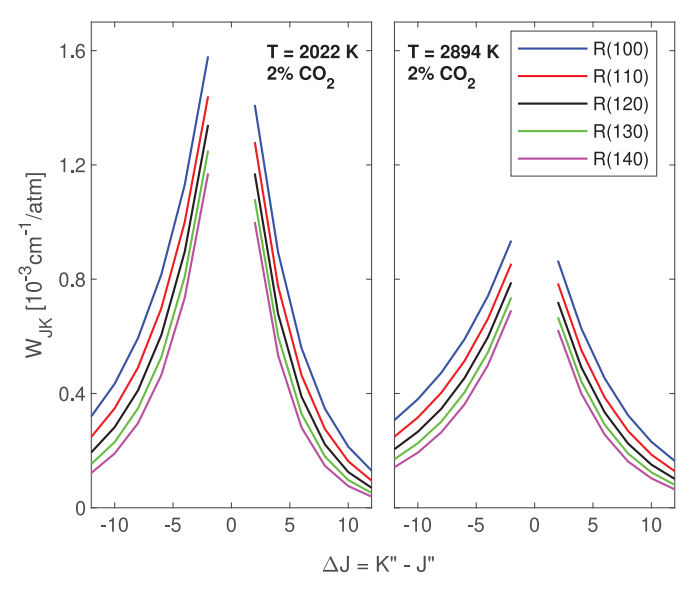


**Fig. 9.**  $W_{JK}$  given by the MEG model, from selected initial states J''=100, 110, 120, 130, and 140 to final K'' states, plotted as  $\Delta J = K'' - J''$ .

ments of the relaxation matrix,  $W_{JK}$ , which are proportional to the state-to-state transfer rates,  $R_{J''\to K''}$ , for select transitions given by the line mixing model at two conditions. In this bandhead, similar to others [35,59], we observe that  $R_{J''\to K''}$  decays as  $\Delta J$  increases, which may be interpreted as collision-induced transfers across larger differences in rotational levels requiring more energy. Fig. 9 illustrates that at higher temperatures, the population transfers from larger  $\Delta J$  become more significant. This can be described through Eq. (13). Notably, the relaxation matrix scales linearly with pressure, but the relative probability of collision-induced transfers between a given  $\Delta J$  is only dependent on temperature. As shown here and similar to our previous line-mixing study [35], at very high temperatures (> 2500 K), population transfers with  $\Delta J > \pm 1$  significantly contribute to the population redistribution in the bandhead.

With the MEG law coefficients inferred empirically at various conditions, the temperature dependence of  $a_1(T)$  was found through Eq. (14) by fitting experimental data at different temperatures, while holding  $a_2$  and  $a_3$  constant. The temperature dependence of the relaxation matrix is captured in Fig. 10 for CO2-Ar collisions. Notably, the temperature exponents for the off-diagonal components of the relaxation matrix are larger than those of the corresponding broadening coefficients. For  $CO_2$ -Ar collisions,  $a_2$ and  $a_3$  were obtained at 2571 K and 58.3 atm with  $a_1$  reported at a reference temperature of  $T_0 = 1200$  K. The reported MEG law coefficients can be found in Table 2. Importantly, the  $W_{IK}$  elements proportional to the specific transfer rates obtained by the reported MEG law coefficients do not completely sum up to the broadening coefficient (as shown in Eq. (11)) due to either the  $A_{RR}$  factor being less than unity or other state-changing collisions outside of the domain considered. For a given rovibrational line, the proxy transfer rates for the grouping of lines considered here summed to a typical value of approximately 70% of the corresponding broadening coefficient. As such, caution should be exercised in using this

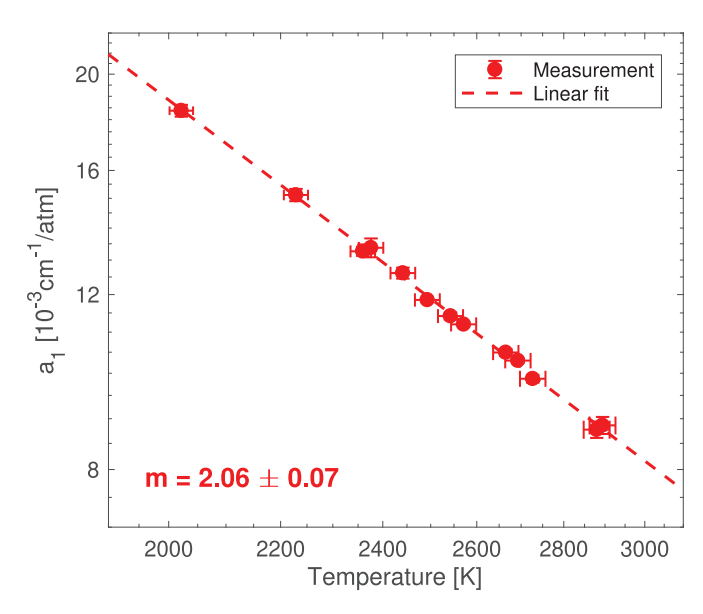


**Fig. 10.** Best-fit determinations of  $a_1$  for different temperatures (markers) with power law fits (dashed line) for  $CO_2$ -Ar collisional line mixing.

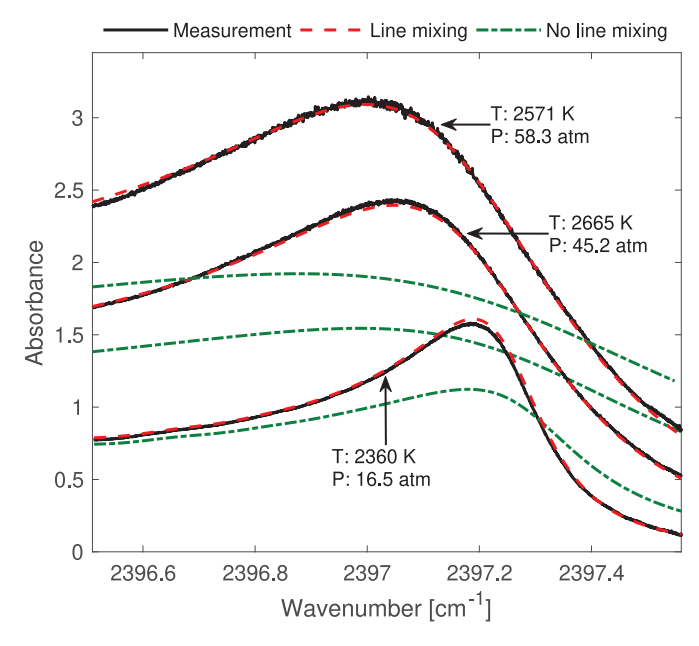


**Fig. 11.** CO<sub>2</sub>-Ar: measured spectral absorbance compared to the developed MEG model used capture line-mixing effects over a range of pressures. The simulated spectral absorbance with no line mixing is illustrated for reference.

relaxation matrix beyond modeling the target absorption spectra, as the real off-diagonal absolute values have not been normalized.

With an established temperature dependence for  $W_{JK}$  and  $\gamma_J$ , the target bandhead spectra can be simulated over a wide range of temperatures and pressures. To validate the pressure scalability and accuracy of the line mixing model, a series of shock tube experiments were conducted from 16.5–58.3 atm for 2% CO<sub>2</sub>/Ar at similar temperatures, respectively, as shown in Fig. 11. At all con-

ditions, the line mixing model exhibits excellent agreement with the measured absorbance spectra.

#### 5. Conclusion

Ar-broadening coefficients and temperature-dependent exponents have been reported for mid-wave infrared CO2 transitions (I = 99-145) in the  $v_3(0 \rightarrow 1)$  fundamental bands near 4.2 µm. Experiments were conducted over a wide range of temperatures, 1200-3000 K, utilizing a shock tube facility. To the authors' knowledge, this work represents the first experimental study of these very high rotational energy transitions (E'' = 3920-8090 cm<sup>-1</sup>), extending the spectroscopic knowledge base of temperature-dependent broadening for CO<sub>2</sub>. With broadening parameters established, a modified exponential gap model was developed to capture the thermodynamic scaling of the relaxation matrix, proportional to state-specific collisional transfer rates associated with line mixing. The line-mixing model developed in this work is shown to accurately simulate the bandhead spectral domain (2395-2398 cm<sup>-1</sup>) over a wide range of temperatures and pressures, 1200-3000 K and 16.5-58.3 atm, relevant to combustion and planetary entry.

#### **CRediT author statement**

All authors contributed equally.

#### **Declaration of Competing Interest**

The authors declare no conflicts of interest.

#### Acknowledgements

This work was supported by the U.S. National Science Foundation, Award No. 1752516, and by the Air Force Research Laboratory under Award No. 16-EPA-RQ-09. Supplementary support was provided by the Air Force Office of Scientific Research (AFOSR) Young Investigator Program (YIP) award no. FA9550-19-1-0062 with Dr. Chiping Li as Program Officer. FAB acknowledges support from the Eugene V. Cota-Robles Fellowship. DIP is supported in part by NSF AGEP Award No. 1306683. The authors acknowledge the experimental assistance of China G. Hagström in the shock tube experiments.

# Appendix A. Uncertainty analysis

The uncertainty analysis presented here follows the analysis presented in the Appendix of Bendana et al [35], with added discussion for inferring the properties for the lines other than those which were directly measured. The broadening parameters reported in Table 1 and the MEG law coefficients reported in Table 2 are provided with uncertainty estimates, the calculations of which are detailed in this Appendix. Unless otherwise noted, we follow the Taylor series method (TSM) of uncertainty propagation [60], in which the uncertainty of a variable r,  $\Delta r$ , is given by:

$$(\Delta r)^2 = \left(\frac{\partial r}{\partial x_1} \Delta x_1\right)^2 + \left(\frac{\partial r}{\partial x_2} \Delta x_2\right)^2 + \cdots \tag{A.1}$$

where  $x_i$  are dependent variables and  $\Delta x_i$  are their respective uncertainties.

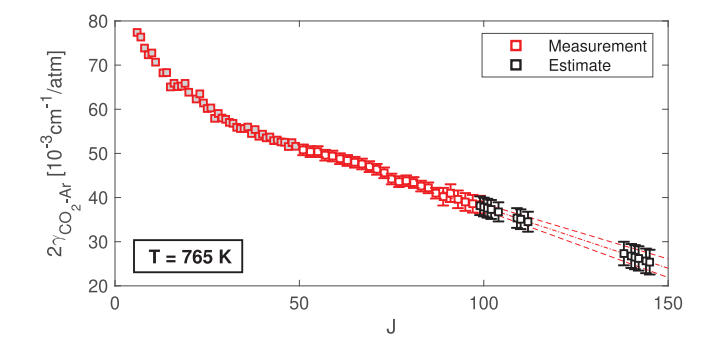


**Fig. A1.** Estimation of  $\gamma$  and  $\Delta \gamma$  at 765 K for high J transitions with measurements of Thibault [24]. Measured values (open red markers with error bars) used in regression (dashed-dot line) shown with regression uncertainty (dashed lines) and estimated values (open black markers with error bars).

# A1. Thermodynamic state variables

The parameters we report are determined from measurements made at various thermodynamic conditions, uncertainties of which ultimately affect the temperature- and pressure-dependence of the associated models.

In this study, uncertainty in pressure is dominated by uncertainty in the reflected shock pressure  $\Delta P_5$  due to uncertainties in the inputs to the normal shock relations. Likewise, there is uncertainty in the reflected shock temperature,  $\Delta T_5$ . For the sake of brevity, the uncertainties  $\Delta P_5$  and  $\Delta T_5$  will not be discussed here in further detail; however, we note that significant contributors include uncertainties in the composition of the driven gas (from the barometric mixture preparation), uncertainties in the time-of-arrival measurements that determine shock velocity, and small uncertainties in the initial pressure  $P_1$  and temperature  $T_1$ . Further information regarding uncertainties in reflected shock conditions can be found in the work by Campbell et al. [52].

# A2. Broadening coefficient

The uncertainties in collisional broadening coefficient  $\gamma_{A-B}(T_0)$  (for absorber A by perturber B),  $\Delta\gamma_{A-B}(T_0)$ , and temperature-dependent exponent,  $\Delta n_{A-B}$ , are determined by applying a linear regression to the natural logarithm of Eq. (6). In this case, the standard errors of the slopes and intercepts of the fitted lines are  $\Delta n_{A-B}$  and  $\Delta\gamma_{A-B}(T_0)$ , respectively. In our linear regressions, we follow the approach of York et al. [61], incorporating variable uncertainties in both x and y to provide slope and intercept standard errors more reflective of variable measurement quality amongst the data. This allows us to utilize measurements from both the shock tube described in this manuscript as well as values estimated from the work of Thibault [24] in the same regression (as shown in Fig. 6), despite that each of the experiments utilized a different facility and has different measurement uncertainties.

As mentioned in Section 4.1, we estimated  $\gamma$  for high J transitions at 765 K by performing a linear regression on values of  $\gamma$  reported by Thibault [24] validated for lower J transitions (J=51-100). This estimate assumes a linear dependence of  $\gamma$  on J for  $J \geq 51$ . The regression, which is weighted according to the reported measurement uncertainty, is shown in Fig. A.12. Since the data are extrapolated, uncertainties in estimated  $\gamma$ ,  $\Delta \gamma$ , are conservatively calculated by summing in quadrature the nearest reported measurement uncertainty ( $\Delta \gamma_{meas}$  for J=100) and the variation resulting from uncertainty in the linear regression,  $\Delta \gamma_{reg}$ :

$$\Delta \gamma_{J \ge 100} = \sqrt{(\Delta \gamma_{meas})^2 + (\Delta \gamma_{reg})^2}$$
 (A.2)

Values of  $\Delta \gamma_{reg}$  at 765 K for J=101-145 (examples shown in Fig. 6) are determined by varying the possible regressions to de-

termine a variation in possible  $\gamma$  which still reproduce measured  $\gamma$  for J=51–100 constrained to within the  $2\sigma$  reported measurement uncertainty. This span is noted by dashed lines in Fig. A.12.

 $\Delta \gamma_{A-B}(T_0)$  and  $\Delta n_{A-B}$  have uncertainty dependence on  $\Delta T$  (discussed previously) and  $\Delta \gamma_{A-B}(T)$ . We can determine  $\Delta \gamma_{A-B}(T)$  by applying Eqs. (A.1) to (5) after rearranging to solve for  $\gamma_{A-B}(T)$ :

$$\left(\frac{\Delta \gamma_{A-B}(T)}{\gamma_{A-B}(T)}\right)^{2} = \left(\frac{\Delta(\Delta \nu_{C})}{2PX_{B}}\right)^{2} + \left(\frac{\Delta \nu_{C} \Delta P}{2P^{2}X_{B}}\right)^{2} + \left(\frac{\Delta \nu_{C} \Delta X_{B}}{2PX_{B}^{2}} - \frac{\Delta X_{B}}{X_{B}} \sum_{C} X_{C} \gamma_{A-C}(T)\right)^{2} + \left(\frac{1}{X_{B}} \sum_{C} \Delta X_{C} \gamma_{A-C}(T)\right)^{2} + \left(\frac{1}{X_{B}} \sum_{C} X_{C} \Delta \gamma_{A-C}(T)\right)^{2} \tag{A.3}$$

Eq. (A.3) describes the uncertainty dependence of the broadening coefficient of absorber A by perturber B,  $\gamma_{A-B}(T)$ , on the uncertainties in collisional width  $\Delta \nu_C$ , total pressure P, mole fraction of perturber B,  $X_B$ , and broadening influences of any other perturbers C (which includes self-broadening by A). When considering only a single perturber B, as in this study, C = A to account for the influence of self-broadening.  $\Delta P$  is determined from  $\Delta P_5$ , and mole fraction uncertainties  $\Delta X_i$  are determined based on the barometric mixture preparation uncertainties. Collisional width  $\Delta \nu_C$  is determined from a Voigt fit of the measured absorbance spectra, and so  $\Delta(\Delta \nu_C)$  is estimated by multiplying the maximum residual of the Voigt fit by  $\Delta \nu_C$ , typically less than 3%.

Thus, the uncertainty dependencies of  $\Delta\gamma_{A-B}(T_0)$  and  $\Delta n_{A-B}$  are all accounted for. For interpolated values of  $\gamma_{A-B}(T)$  between J of 113–137 which were not directly measured (noted with superscript  $^a$  in Table 1),  $\Delta\gamma_{A-B}(T)/\gamma_{A-B}(T)$  was assumed to be the same as the largest  $\Delta\gamma_{A-B}(T)/\gamma_{A-B}(T)$  calculated for directly measured transitions; in this study, approximately 9%.

# A3. MEG law coefficients

The MEG coefficients  $a_1(T)$ ,  $a_2$ , and  $a_3$  for each experiment are empirically determined by a nonlinear least-squares fit so their uncertainties cannot be interpreted as meaningfully through physical relationships as described by Eq. (A.1). Therefore, we estimate uncertainties for these coefficients in a manner consistent with how the model will be used; i.e., to accurately simulate absorption spectra in the range of thermodynamic conditions described in this work. The uncertainties in  $a_1(T)$ ,  $a_2$  and  $a_3$  for each high-pressure shock tube experiment were inferred by varying the wavenumber range over which the least-squares fit described in Section 4.2 was implemented. The differences between the values of  $a_i$  determined from simulating the wavelength range of the measured experiment (2396–2398 cm<sup>-1</sup>) and the values of  $a_i$  determined from simulating the wavelength range of the  $(00^00 \rightarrow 00^01)$  band before overlapping with the other band (2385–2398 cm<sup>-1</sup>) were taken to conservatively estimate  $\Delta a_i$ . This represents the uncertainty associated with using experimental data gathered from a limited spectral range to model the line mixing behavior of the entire band.

The uncertainties for  $a_1(T)$ ,  $\Delta a_1(T)$ , are shown as error bars in Fig. 10. Together with  $\Delta T$ , these are used in the linear regression determination of  $a_1(T_0)$  and m to obtain their respective uncertainties  $\Delta a_1(T_0)$  and  $\Delta m$  using the same approach of York et al. [61] as described for  $\Delta \gamma_{A-B}(T_0)$  and  $\Delta n_{A-B}$ .

# Supplementary material

Supplementary material associated with this article can be found, in the online version, at 10.1016/j.jgsrt.2020.107135.

#### References

- Snels M, Stefani S, Grassi D, Piccioni G, Adriani A. Carbon dioxide opacity of the Venus atmosphere. Planet Space Sci 2014;103:347–54. doi:10.1016/j.pss.2014. 08.002
- [2] Barbu TL, Vinogradov I, Durry G, Korablev O, Chassefière E, Bertaux J-L. TDLAS a laser diode sensor for the in situ monitoring of H<sub>2</sub>O, CO<sub>2</sub> and their isotopes in the Martian atmosphere. Adv Space Res 2006;38(4):718–25. doi:10.1016/j. asr.2005.04.049.
- [3] Spearrin RM, Goldenstein CS, Jeffries JB, Hanson RK. Fiber-coupled 2.7 μm laser absorption sensor for CO<sub>2</sub> in harsh combustion environments. Meas Sci Technol 2013;24(5):055107. doi:10.1088/0957-0233/24/5/055107.
- [4] Park C, Howe JT, Jaffe RL, Candler GV. Review of chemical-kinetic problems of future NASA missions, II: Mars entries. J Thermophys Heat Transf 1994;8(1):9– 23. doi:10.2514/3.496.
- [5] Takayanagi H, Lemal A, Nomura S, Fujita K. Measurements of Carbon Dioxide Nonequilibrium Infrared Radiation in Shocked and Expanded Flows. J Thermophys Heat Transf 2018;32(2):483–94. doi:10.2514/1.T5200.
- [6] Spearrin RM, Goldenstein CS, Schultz IA, Jeffries JB, Hanson RK. Simultaneous sensing of temperature, CO, and CO<sub>2</sub> in a scramjet combustor using quantum cascade laser absorption spectroscopy. Appl Phys B 2014;117(2):689–98. doi:10. 1007/s00340-014-5884-0.
- [7] Villarreal R, Varghese PL. Frequency-resolved absorption tomography with tunable diode lasers. Appl Opt 2005;44(31):6786–95. doi:10.1364/AO.44.006786.
- [8] Girard JJ, Spearrin RM, Goldenstein CS, Hanson RK. Compact optical probe for flame temperature and carbon dioxide using interband cascade laser absorption near 4.2m. Combust Flame 2017;178:158–67. doi:10.1016/j.combustflame. 2017.01.007.
- [9] Liu X, Zhang G, Huang Y, Wang Y, Qi F. Two-dimensional temperature and carbon dioxide concentration profiles in atmospheric laminar diffusion flames measured by mid-infrared direct absorption spectroscopy at 4.2 μm. Appl Phys B 2018;124(4):61. doi: 10.1007/s00340-018-6930-0.
- [10] Wei C, Pineda DI, Paxton L, Egolfopoulos FN, Spearrin RM. Mid-infrared laser absorption tomography for quantitative 2D thermochemistry measurements in premixed jet flames. Appl Phys B 2018;124(6):123. doi:10.1007/ s00340-018-6984-z.
- [11] Wei C, Pineda DI, Goldenstein CS, Spearrin RM. Tomographic laser absorption imaging of combustion species and temperature in the mid-wave infrared. Opt Express 2018;26(16):20944. doi:10.1364/OE.26.020944.
- [12] Tancin RJ, Chang Z, Radhakrishna V, Gu M, Lucht RP, Goldenstein CS. Ultra-fast Laser Absorption Spectroscopy in the Mid-Infrared for Measuring Temperature and Species in Combustion Gases. In: AIAA Scitech 2020 Forum. Reston, Virginia: American Institute of Aeronautics and Astronautics; 2020. p. 1–9. doi:10.2514/6.2020-0517. ISBN 978-1-62410-595-1
- [13] Spearrin RM, Ren W, Jeffries JB, Hanson RK. Multi-band infrared CO<sub>2</sub> absorption sensor for sensitive temperature and species measurements in high-temperature gases. Appl Phys B 2014;116(4):855–65. doi:10.1007/s00340-014-5772-7.
- [14] Ren W, Spearrin RM, Davidson DF, Hanson RK. Experimental and Modeling Study of the Thermal Decomposition of C3C5 Ethyl Esters Behind Reflected Shock Waves. J Phys Chem A 2014;118(10):1785–98. doi:10.1021/jp411766b.
- [15] Javed T, Nasir EF, Es-Sebbar ET, Farooq A. A comparative study of the oxidation characteristics of two gasoline fuels and an n-heptane/iso-octane surrogate mixture. Fuel 2015;140:201-8. doi:10.1016/j.fuel.2014.09.095.
- [16] Ren W, Lam KY, Davidson DF, Hanson RK, Yang X. Pyrolysis and oxidation of methyl acetate in a shock tube: A multi-species time-history study. Proc Combust Inst 2017;36(1):255-64. doi:10.1016/j.proci.2016.05.002.
- [17] Lee DD, Bendana FA, Nair AP, Spearrin RM, Danczyk SA, Hargus WA. Laser absorption of carbon dioxide at the vibrational bandhead near 4.2 μm in high-pressure rocket combustion environments. AIAA Scitech 2020 Forum. Reston, Virginia: American Institute of Aeronautics and Astronautics; 2020. doi:10.2514/6.2020-0298. ISBN 978-1-62410-595-1
- [18] Hartmann J-M, Tran H, Armante R, Boulet C, Campargue A, Forget F, et al. Recent advances in collisional effects on spectra of molecular gases and their practical consequences. J Quant Spectrosc Radiat Transf 2018;213:178–227. doi:10.1016/j.jqsrt.2018.03.016.
- [19] Brownsword RA, Salh JS, Smith IWM. Collision broadening of CO<sub>2</sub> transitions in the region of 4.3 μm. Effects of broadening gas (He, Ar and N<sub>2</sub>), rovibrational states and temperature. J Chem Soc Faraday Trans 1995;91(2):191–5. doi:10. 1039/FT9959100191.
- [20] Rachet F, Margottin-Maclou M, Henry A, Valentin A. Q-Branch Line Mixing Effects in the (20<sup>0</sup>0)<sub>1</sub>←01<sup>1</sup>0 and (12<sup>2</sup>0)<sub>1</sub>←01<sup>1</sup>0 Bands of Carbon Dioxide Perturbed by N<sub>2</sub>, O<sub>2</sub>, and Ar and in the 13<sup>1</sup>0←00<sup>0</sup>0 and 13<sup>1</sup>0←01<sup>1</sup>0 Bands of Pure Nitrous Oxide. J Mol Spectrosc 1996;175(2):315–26. doi:10.1006/jmsp. 1996.0037.
- [21] Wooldridge MS, Hanson RK, Bowman CT. Argon broadening of the R(48), R(50) and R(52) lines of CO<sub>2</sub> in the (00<sup>0</sup>1)←(00<sup>0</sup>0) band. J Quant Spectrosc Radiat Transf 1997;57(3):425–34. doi:10.1016/S0022-4073(96)00074-X.
- [22] Thibault F, Boissoles J, Boulet C, Ozanne L, Bouanich JP, Roche CF, Hutson JM. Energy corrected sudden calculations of linewidths and line shapes based

- on coupled states cross sections: The test case of CO<sub>2</sub>-argon. J Chem Phys 1998:109(15):6338-45. doi:10.1063/1.477187.
- [23] Khalil B, Thibault F, Boissoles J. Argon-broadened CO<sub>2</sub> linewidths at high J values. Chem Phys Lett 1998;284(3-4):230-4. doi:10.1016/S0009-2614(97) 01412-7
- [24] Thibault F, Calil B, Buldyreva J, Chrysos M, Hartmann J-M, Bouanich J-P. Experimental and theoretical CO<sub>2</sub>-Ar pressure-broadening cross sections and their temperature dependence. Phys Chem Chem Phys 2001;3(18):3924–33. doi:10.1039/b103625b.
- [25] Mulvihill CR, Petersen EL. High-temperature argon broadening of CO<sub>2</sub> near 2190 cm<sup>-1</sup> in a shock tube. Appl Phys B 2017;123(10):255. doi:10.1007/ s00340-017-6830-8.
- [26] Hartmann JM, Boulet C, Robert D. Collisional effects on Molecular Spectra. Elsevier; 2008. doi:10.1016/B978-0-444-52017-3.X0001-5. ISBN 9780444520173
- sevier; 2008. doi:10.1016/B978-0-444-52017-3.X0001-5. ISBN 9780444520173
   [27] Cousin C, Le Doucen R, Boulet C, Henry A, Robert D. Line coupling in the temperature and frequency dependences of absorption in the microwindows of the 4.3 μm CO<sub>2</sub> band. J Quant Spectrosc Radiat Transf 1986;36(6):521-38. doi:10.1016/0022-4073(86)90125-1.
- [28] Perrin MY, Hartmann JM. Temperature-dependent measurements and modeling of absorption by CO<sub>2</sub>-N<sub>2</sub> mixtures in the far line-wings of the 4.3 μm CO<sub>2</sub> band. J Quant Spectrosc Radiat Transf 1989;42(4):311–17. doi:10.1016/0022-4073(89)90077-0.
- [29] Boissoles J, Menoux V, Le Doucen R, Boulet C, Robert D. Collisionally induced population transfer effect in infrared absorption spectra. II. The wing of the Ar-broadened ν<sub>3</sub> band of CO<sub>2</sub>. J Chem Phys 1989;91(4):2163–71. doi:10.1063/ 1.457024.
- [30] Ozanne L, Ma Q, Nguyen-Van-Thanh, Brodbeck C, Bouanich JP, Hartmann JM, Boulet C, Tipping RH. Line-mixing, finite duration of collision, vibrational shift, and non-linear density effects in the ν<sub>3</sub> and 3ν<sub>3</sub> bands of CO<sub>2</sub> perturbed by Ar up to 1000 bar. J Quant Spectrosc Radiat Transf 1997;58(2):261–77. doi:10. 1016/S0022-4073/97)00007-1.
- [31] Tran H, Boulet C, Stefani S, Snels M, Piccioni G. Measurements and modeling of high pressure pure CO<sub>2</sub> spectra from 750 to 8500 cm<sup>-1</sup>. I-central and wing regions of the allowed vibrational bands. J Quant Spectrosc Radiat Transf 2011;112(6):925–36. doi:10.1016/j.jqsrt.2010.11.021.
- [32] Lamouroux J, Régalia L, Thomas X, Vander Auwera J, Gamache RR, Hartmann JM. CO<sub>2</sub> line-mixing database and software update and its tests in the 2.1  $\mu$ m and 4.3  $\mu$ m regions. J Quant Spectrosc Radiat Transf 2015;151:88–96. doi:10.1016/j.jqsrt.2014.09.017.
- [33] Sagan C. The Planet Venus: Recent observations shed light on the atmosphere, surface, and possible biology of the nearest planet. Science 1961;133(3456):849–58. doi:10.1126/science.133.3456.849.
- [34] Hanson RK, Spearrin RM, Goldenstein CS. Spectroscopy and Optical Diagnostics for Gases. Springer; 2016. doi:10.1007/978-3-319-23252-2. ISBN 978-3-319-23252-2
- [35] Bendana FA, Lee DD, Wei C, Pineda DI, Spearrin RM. Line mixing and broadening in the ν(1→3) first overtone bandhead of carbon monoxide at high temperatures and high pressures. J Quant Spectrosc Radiat Transf 2019;239:106636. doi:10.1016/j.jqsrt.2019.106636.
- [36] Hill TL. An Introduction to Statistical Thermodynamics. Addison-Wesley Publishing Co; 1960. ISBN 9780486652429
- [37] Fano U. Pressure Broadening as a Prototype of Relaxation. Phys Rev 1963;131(1):259–68. doi:10.1103/PhysRev.131.259.
- [38] Baranger M. Problem of Overlapping Lines in the Theory of Pressure Broadening. Phys Rev 1958;111(2):494–504. doi:10.1103/PhysRev.111.494.
- [39] Gordon RG, McGinnis RP. Line Shapes in Molecular Spectra. J Chem Phys 1968;49(5):2455–6. doi:10.1063/1.1670429.
- [40] Gordon RG. Semiclassical Theory of Spectra and Relaxation in Molecular Gases. J Chem Phys 1966;45(5):1649–55. doi:10.1063/1.1727808.
- [41] Ben-Reuven A. Impact Broadening of Microwave Spectra. Phys Rev 1966;145(1):7–22. doi:10.1103/PhysRev.145.7.

- [42] Lévy A, Lacome N, Chackerian C. Collisional Line Mixing. In: Spectroscopy of the Earth's atmosphere and interstellar medium. Elsevier; 1992. p. 261–337. doi:10.1016/B978-0-12-580645-9.50008-3. ISBN 0125806450
- [43] Koszykowski ML, Rahn LA, Palmer RE, Coltrin ME. Theoretical and experimental studies of high-resolution inverse Raman spectra of N<sub>2</sub> at 1–10 atm. J Phys Chem 1987;91(1):41–6. doi:10.1021/j100285a012.
- [44] Rahn L, Palmer R, Koszykowski M, Greenhalgh D. Comparison of rotationally inelastic collision models for Q-branch Raman spectra of N<sub>2</sub>. Chem Phys Lett 1987;133(6):513–16. doi:10.1016/0009-2614(87)80069-6.
- [45] Hirschfelder JO, Curtiss CF, Bird RB. Molecular Theory of Gases and Liquids. 2nd ed. New York: John Wiley & Sons, Inc.; 1964.
- [46] Pine AS, Looney JP. Self-broadening and line mixing in HCN Q branches. J Chem Phys 1992;96(3):1704–14. doi:10.1063/1.462125.
- [47] Rosasco GJ, Rahn LA, Hurst WS, Palmer RE, Dohne SM. Measurement and prediction of Raman Q branch line self-broadening coefficients for CO from 400 to 1500 k. J Chem Phys 1989;90(8):4059–68. doi:10.1063/1.455764.
- [48] Lavorel B, Millot G, Saint-Loup R, Berger H, Bonamy L, Bonamy J, Robert D. Study of collisional effects on band shapes of the  $v_1/2v_2$  Fermi dyad in CO<sub>2</sub> gas with stimulated Raman spectroscopy. II. Simultaneous line mixing and Dicke narrowing in the  $v_1$  band. J Chem Phys 1990;93(4):2185–91. doi:10.1063/1. 459050
- [49] Margottin-Maclou M, Henry A, Valentin A. Line mixing in the Q branches of the  $\nu_1+\nu_2$  band of nitrous oxide and of the  $(11^10)_l \leftarrow (02^20)$  band of carbon dioxide. Chem Phys 1992;96(3):1715–23. doi:10.1063/1.462126.
- [50] Steinfeld JI, Ruttenberg P, Millot G, Fanjoux G, Lavorel B. Scaling laws for inelastic collision processes in diatomic molecules. J Phys Chem 1991;95(24):9638–47. doi:10.1021/j100177a010.
- [51] Pineda DI, Bendana FA, Schwarm KK, Spearrin RM. Multi-isotopologue laser absorption spectroscopy of carbon monoxide for high-temperature chemical kinetic studies of fuel mixtures. Combust Flame 2019;207:379–90. doi:10.1016/ i.combustflame.2019.05.030.
- [52] Campbell MF, Owen KG, Davidson DF, Hanson RK. Dependence of Calculated Postshock Thermodynamic Variables on Vibrational Equilibrium and Input Uncertainty. J Thermophys Heat Transf 2017;31(3):586–608. doi:10.2514/1.T4952.
- [53] Gamache RR, Lamouroux J. The vibrational dependence of half-widths of CO<sub>2</sub> transitions broadened by N<sub>2</sub>, O<sub>2</sub>, air, and CO<sub>2</sub>. J Quant Spectrosc Radiat Transf 2013;117:93–103. doi:10.1016/j.jqsrt.2012.10.028.
- [54] Gamache RR, Lamouroux J, Blot-Lafon V, Lopes E. An intercomparison of measured pressure-broadening, pressure shifting parameters of carbon dioxide and their temperature dependence. J Quant Spectrosc Radiat Transf 2014;135:30–43. doi:10.1016/j.jqsrt.2013.11.001.
- [55] Li H, Owens ZC, Davidson DF, Hanson RK. A simple reactive gasdynamic model for the computation of gas temperature and species concentrations behind reflected shock waves. Int J Chem Kinet 2008;40(4):189–98. doi:10.1002/kin. 20305.
- [56] Varghese PL, Hanson RK. Collisional narrowing effects on spectral line shapes measured at high resolution. Appl Opt 1984;23(14):2376. doi:10.1364/AO.23. 002376.
- [57] Rothman LS, Gordon IE, Barber RJ, Dothe H, Gamache RR, Goldman A, Perevalov VI, Tashkun SA, Tennyson J. HITEMP, the high-temperature molecular spectroscopic database. J Quant Spectrosc Radiat Transf 2010;111(15):2139–50. doi:10.1016/j.jqsrt.2010.05.001.
- [58] Gordon I, Rothman L, Hill C, Kochanov R, Tan Y, Bernath P, et al. The HI-TRAN2016 molecular spectroscopic database. J Quant Spectrosc Radiat Transf 2017;203:3-69. doi:10.1016/j.jqsrt.2017.06.038.
- [59] Romanini D, Lehmann KK. Linemixing in the 106←000 overtone transition of HCN. J Chem Phys 1996;105(1):81–8. doi:10.1063/1.471883.
- [60] Coleman HW, Steele WG. Experimentation, Validation, and Uncertainty Analysis for Engineers. 3rd ed. Hoboken, NJ, USA: John Wiley & Sons, Inc.; 2009.
- [61] York D, Evensen NM, Martnez ML, De Basabe Delgado J. Unified equations for the slope, intercept, and standard errors of the best straight line. Am J Phys 2004;72(3):367–75. doi:10.1119/1.1632486.